# Well-Defined Star-Shaped Conjugated Macroelectrolytes as Efficient Electron-Collecting Interlayer for Inverted Polymer Solar Cells

Weidong Xu,[†] Zhipeng Kan,[‡] Tengling Ye,[‡,||] Li Zhao,[†] Wen-Yong Lai,*[,†] Ruidong Xia,*[,†] Guglielmo Lanzani,[‡] Panagiotis E. Keivanidis,*[,‡,⊥] and Wei Huang*[,†,§]

[†]Key Laboratory for Organic Electronics and Information Displays & Institute of Advanced Materials(IAM), Jiangsu National Synergistic Innovation Center for Advanced Materials (SICAM), Nanjing University of Posts & Telecommunications, 9 Wenyuan Road, Nanjing 210023, China

[‡]Center for Nano Science and Technology@PoliMi, Istituto Italiano di Tecnologlia, via G. Pascoli 70/3, I-20133 Milano, Italy

[§]Key Laboratory of Flexible Electronics (KLOFE) & Institute of Advanced Materials (IAM), Jiangsu National Synergistic Innovation Center for Advanced Materials (SICAM), Nanjing Tech University (NanjingTech), 30 South Puzhu Road, Nanjing 211816, China

**S** *Supporting Information*

**ABSTRACT:** A star-shaped monodisperse conjugated macroelectrolyte grafted with cationic side chains, TrNBr, was designed, synthesized, and utilized as efficient electron-collecting cathode interlayers for inverted polymer solar cells. A neutral one composed of identical star-shaped conjugated backbone, TrOH, was also investigated for comparison. The surface properties and the function as interfacial layers on modulating the work function of bottom electrode (indium tin oxide) were systematically studied. Both interfacial electron-selective materials show strongly thickness-dependent performance for inverted polymer solar cells, and the best performance could be achieved via optimizing the thickness with 2.4 nm of TrNBr and 8.7 nm of TrOH. Parallel investigations of optimized TrNBr and TrOH interlayer in inverted architecture with active blend layer of poly(3-hexylthiophene):indene$-C_{60}$ bisadduct (P3HT:ICBA) demonstrated a remarkable power conversion efficiency (PCE) enhancement (PCE of 4.88% for TrNBr and 4.74% for TrOH) in comparison with those of conventional noninverted devices using Ca/Al cathodes (3.94%) and inverted devices with sol−gel ZnO buffer layer (4.21%). In addition, the inverted devices using the TrNBr and TrOH interlayer exhibited improved device stability in contrast to conventional noninverted devices using Ca/Al cathodes.

**KEYWORDS:** *inverted polymer solar cells, cathode interlayer, star-shaped molecule, conjugated polyeletrolytes*
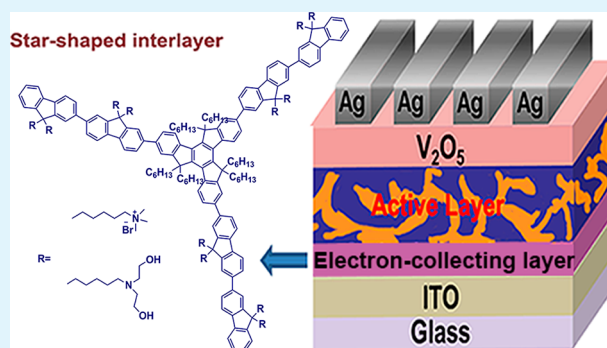
## 1. INTRODUCTION

Organic photovoltaic technology is a promising method to utilize solar energy because of its low-cost, high throughput fabrication, lightweight physical characteristics, and the lucrative possibility of integration directly into flexible devices. During the past decade, the most widely investigated organic photovoltaic device architecture is a bulk heterojunction (BHJ) active layer on top of a poly(3,4-ethylenedioxythiophene):poly(polystyrene sulfonic acid) (PEDOT:PSS) hole-collecting (HC) layer coated on indium tin oxide (ITO), capped by a low-work-function metal electron-collecting (EC) layer such as Ca, Ba, etc.[1−6] These kinds of devices suffer from poor air stability and short operational lifetime, and thus strict encapsulation is required to prevent degradation under oxygen and moisture atomosphere.[7,8] Considering the practical aspects for commercialization, inverted polymer solar cells (*i*PSCs) consisting of an organic semiconductor layer between the bottom ITO EC layer and the air-stable high-work-function metal HC electrodes such as Au

and Ag, have been confirmed as one promising approach for long-term stability by avoiding the use of environmental unstable metals and acidic PEDOT:PSS.[9,10] Another reason for exploring the BHJ films in *i*PSCs is that it undergoes the desired vertical phase separation with a composition gradient that favor charge transport and collection, which can significantly improve photovoltaic device performance.[11] In typical inverted geometry, a high work function metal oxide (MO) layer (e.g., $V_2O_5$ and $MoO_3$) is used as the hole selective layer and optical spacer between the active layer and the HC-electrode.[12,13] At the EC-electrode side, bare ITO is not an ideal electron extraction electrode because its high work function (~4.7 eV) hinders the ohmic contact with the lowest unoccupied molecular orbital (LUMO) of the fullerene. To achieve high-performance inverted devices, interface modifica-

**Scheme 1**[a]
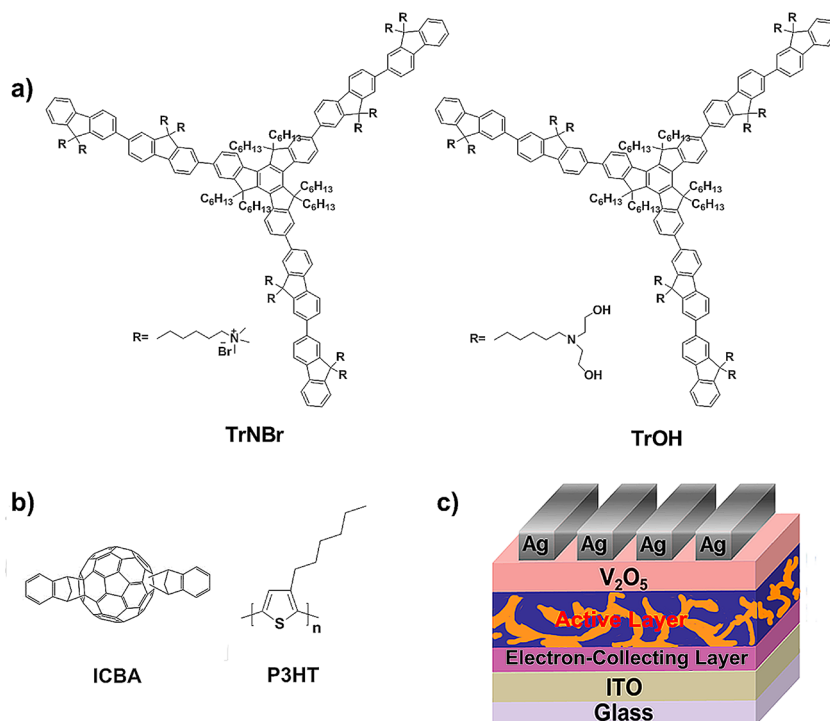


[a]Chemical structures of (a) star-shaped interlayers used in solar cell fabrication; (b) the active layer components employed: electron-donor (P3HT) and -acceptor (ICBA) materials; (c) the inverted device architecture.

tion has been demonstrated as an effective way in reducing the work function of ITO and improving electron extraction ability. Various kinds of interfacial materials including n-type MOs (ZnO, $TiO_x$, $MoO_3$–Al composite),[14−16] alkali-metal compounds,[17,18] cross-linked fullerene,[19] and self-assembled dipole molecules,[20] have been investigated.

In recent reports, it has been demonstrated that incorporating a conjugated polyelectrolyte (CPE) interlayer between the EC electrode and the organic active layer can improve device performance by changing the electronic and orbital interactions at the interfaces.[21−26] The good solubility of CPEs in polar solvents such as water and alcohol offers good opportunities to avoid interfacial mixing upon fabrication of multilayer optoelectronic devices by solution processing, which provide the potential for simple and large area processing in a roll-to-roll or inject printing manufacturing.[27] Spin-coating a thin film of CPEs (tethered with different polar groups such as *N,N*-dimethylamino and ammonium,[28−30] phosphonate,[31] and ethylene oxide[32]) on bare ITO or ITO/MOs can effectively reduce the work function of bottom electrodes and improve the interface contact between the organic active layer and the EC electrodes, leading to high-performance inverted devices.

It was proposed that the excellent performance of CPEs originates mainly from the charged or polar groups on the side chains, which can generate positive interfacial dipole between EC electrodes and organic active layer, leading to raised vacuum level close to that of the electrode.[33] Very recently, a nonconjugated polyelectrolyte (PEIE) has been reported, and the effect of polar pendant groups has been well-discussed.[34] In contrast, the influence of the π-delocalized structures remain less studied. Chen et al. reported a superbranched CPE interlayer, which demonstrated a distinctive surface morphology and superior performance to linear CPEs in *i*PSCs

efficiency.[35] Very recently, one metallopolymer interlayer with high conductivity and less thickness-dependent performance was developed.[36] These reports encourage the view that the performance of interlayers might be further improved by additional tuning of their chemical structures.

Monodisperse well-defined π-conjugated macromolecules, such as dendrimers and starburst molecules, are well-known for their definite uniform chemical structures, high purity, excellent reproducibility, good solution processability, and generally superior optoelectronic properties.[37−42] Such promising characteristics of monodisperse macromolecules make them rather attractive as novel backbones for cathode interlayers and stand out as a novel series of molecular systems to better understand the structure−function correlations. These have motivated our recent interest in exploring hydrophilic monodisperse starburst conjugated macroelectrolytes (CMEs), which were characterized by a conjugated central core unit with short conjugated arms grafted with polar pendant groups, as interfacial layers for organic electronics. Our recent results showed that such monodisperse starburst CME performed much better than its polymer analogues as electron transport/injection layer for organic light-emitting diodes.[43] Moreover, this kind of material with monodisperse characteristics could also effectively avoid the intractable problems met with their polymer counterparts in terms of molecular weight and polydispersity, catalyst residues, and poor reproducibility; their three-dimensional molecular topology is also of benefit for improving the orthogonal solvent processability.[43] It therefore appears to be a promising candidate for interfacial modification.

In the present study, a novel star-shaped macro-electrolyte grafted with ammonium moiety named TrNBr was successfully synthesized and utilized as an EC interlayer in *i*PSCs with the active blend layer of poly(3-hexylthiophene):indene−$C_{60}$
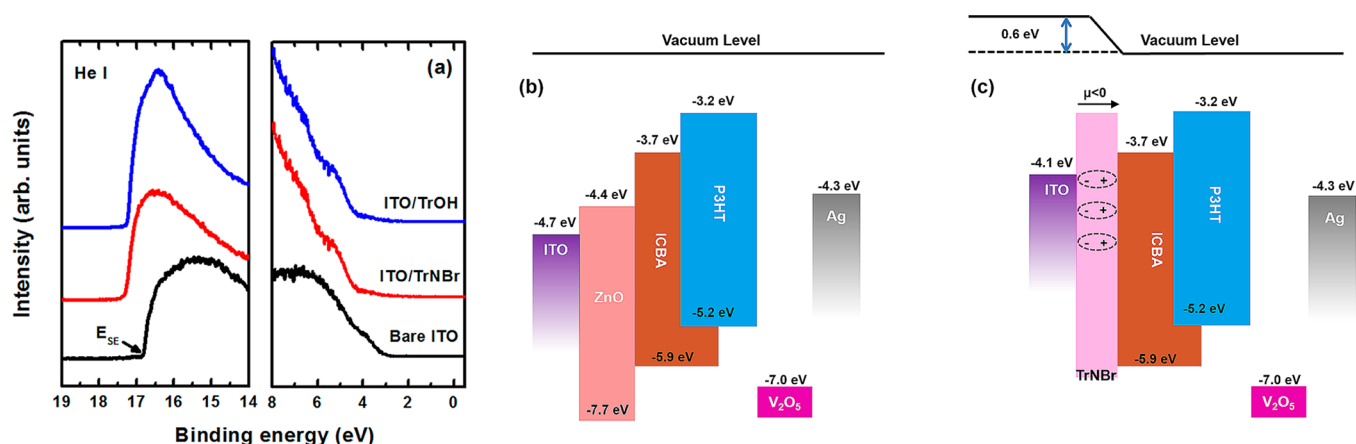
**Figure 1.** (a) UPS for bare ITO and after TrNBr and TrOH deposition (5 nm). (b) Energy-level diagrams of the inverted device components under flat band condition. (c) Illustration of VL shift and reduced work function of ITO electrode after the deposition of star-shaped interlayer (TrNBr). The data for the energy levels except those of TrNBr interlayer are cited from literature.[14,47]

bisadduct (P3HT:ICBA). The high LUMO level of ICBA is of great benefit for achieving large $V_{OC}$ and good device performance in incorporating P3HT as donor.[44] Its counterpart comprising identical star-shaped conjugated backbones with diethanolaminohexyl as side chains (TrOH) was studied as well (see Scheme 1 for the chemical structures and device configuration).[37] Conventional Ca/Al-based devices and inverted geometry with sol−gel-derived ZnO as the EC layer were fabricated as reference devices.[14] We demonstrate that incorporating the star-shaped EC interlayer between the active layer and ITO electrode leads to a significant enhancement of power conversion efficiency (PCE) and stability.

## 2. EXPERIMENTAL DETAILS

NMR spectra were recorded on a Bruker Ultra Shield Plus 400 MHz NMR ([1]H: 400 MHz). The UV−visible absorption and transmittance spectra were recorded using a Shimadzu UV-3600 UV−vis−NIR spectrophotometer. Atomic force microscopy (AFM) measurements of surface morphology were conducted on the Bruker ScanAsyst AFM in auto scan (AC) mode. Film water contact angles were measured with a CAM 200 (KSV Instrument LID), and the photos were taken with a BASLER A602f-2 camera. Ultraviolet photoelectron spectroscopy (UPS) measurements were conducted in a Kratos AXIS Ultra DLD ultrahigh-vacuum (UHV) surface analysis system. UPS analysis with an unfiltered HeI (21.2 eV) gas discharge lamp was performed to characterize the valence states and the vacuum level, showing a total instrumental energy resolution of 100 meV. Small-angle X-ray diffraction pattern (XRD) of the interlayer materials was recorded by Bruker D8 advance.

The glass/ITO substrates were precleaned with acetone, isopropanol, and a special detergent and dried under a flow of dry nitrogen. Before the deposition of the organic layers the ITO substrates were cleaned in $O_2$ plasma for 10 min. Inverted PSCs were fabricated with structure ITO/interlayer/P3HT:ICBA/$V_2O_5$/Ag and conventional PSCs with structure ITO/PEDOT:PSS/P3HT:ICBA/Ca/Al. For the inverted PSCs, TrNBr and TrOH were spin-coated from their various concentration solutions onto pretreated ITO substrates at 2000 rpm baked at 60 °C for 10 min in air. The sol−gel-derived ZnO films were prepared according to the literature.[14] For reference PSC structures, a thin layer (30 nm) of PEDOT:PSS was spin-coated onto pretreated ITO substrates and annealed at 150 °C for 30 min in air.

In all cases, the spin-coated structures were then transferred into a nitrogen-filled glovebox (<0.1 ppm of $O_2$ and $H_2O$). P3HT:ICBA (1:1 by weight, 250 nm thickness) was then spin-coated on top as per from 44 mg/mL $o$-dichlorobenzene ($o$-DCB) solution at 1000 rpm and annealed at 150 °C for 15 min inside glovebox. Top electrodes were

then thermally evaporated through a shadow mask onto the P3HT:ICBA. The 2.0 nm $V_2O_5$ followed by 80 nm Ag or 15 nm Ca followed by 80 nm Al top electrodes were thermally deposited in vacuum at a base pressure of $2 \times 10^{-6}$ Torr. Finally, all the devices were encapsulated in glovebox with the epoxy and hardener (1:1 in volume) mixture and covered with a glass slide. For all devices, the active area of the pixels as defined by the overlap of anode and cathode area was 0.0525 cm$^2$. Eight individual PSC devices were prepared simultaneously on each substrate.

The current density−voltage ($J−V$) characteristics were measured using a Keithley 2400 source measure unit. The photocurrent was measured under AM 1.5G illumination (through the glass substrate) at 100 mW/cm$^2$ using a Newport Thermo Oriel 91192 1000W Solar Simulator. Incident photon conversion efficiency (IPCE) spectra were recorded using the monochromated (Bentham) output from a tungsten halogen lamp calibrated with a Newport UV-181 photodiode; phase-sensitive detection with a lock-in amplifier was used to increase the signal-to-noise ratio.

## 3. RESULTS AND DISCUSSION

The synthetic procedures of TrNBr and TrOH are shown in Scheme S1 in the Supporting Information and were well-described in our previous work.[37] Both TrNBr and TrOH comprise a truxene core and oligofluorene arms, tethered with cationic ammonium groups or neutral diethanolamino polar groups, respectively. One advantage of these dendronized molecules is that they show excellent solubility (more than 30 mg/mL for TrNBr in methanol and 25 mg/mL in ethanol for TrOH) in polar solvents compared to many linear CPE-based interlayers in literature, which is attributed to the effective reduction of aggregation in polar solution due to their multidimensional architectures.[45,46] For TrNBr, a good solubility of nearly 8 mg/mL in water makes it really attractive for the possibility of being solution-processed by aqueous solution. To certify their orthogonal-solvent properties, the optical absorption spectra of these interlayer films before and after rinsing with 1,2-dichlorobenzene ($o$-DCB) were recorded. As shown in the Figure S4 (see Supporting Information), both absorption spectra show no obvious variation, indicating these interlayers will not be damaged by the subsequent active layer solution.

Figure 1a presents UPS data of star-shaped interlayer materials deposited on ITO and of the pristine ITO. The shift of the secondary electron cutoff ($E_{SE}$) in the high binding-energy region after 5 nm of interlayer deposition indicates a

vacuum level (VL) shift of nearly 0.6 and 0.5 eV for TrNBr film and TrOH film, respectively. On the basis of the UPS results, the energy diagrams for BHJ solar cells with the star-shaped EC layer are sketched in Figure 1b,c. The work function of ITO was reduced to 4.1 and 4.2 eV, which is closer to the LUMO level of ICBA (3.7 eV) in contrast to ZnO (4.4 eV).[14] In both cases, the deposition of the interlayer creates a strong dipole at the interface and makes a VL shift, leading an ohmic contact with the LUMO level of ICBA. Therefore, TrNBr and TrOH can be utilized as EC interlayer for $i$PSCs to facilitate transport and collection of photogenerated charge carriers.

Then we investigated the interface properties of these starburst interlayers. Water contact angle ($\theta$) measurements were performed on TrNBr- and TrOH-coated ITO surfaces with various thickness (the spin-coating condition is identical to device fabrication; see Figures S6 and S7, Supporting Information). TrNBr exhibited a strong hydrophilic property with contact angle ranging from 33.9° (0.05 mg/mL, 1.40 ± 0.16 nm) to 21.5° (0.5 mg/mL, 4.8 ± 0.09 nm). Different from its cationic counterpart, TrOH exhibited an amphiphilic property with a relatively larger contact angle from 78.3° (0.25 mg/mL, 5.0 ± 0.11 nm) to 68.6° (1.00 mg/mL, 12.10 ± 0.32 nm). The contact angle of both interlayers was increased with increase of thickness, most probably due to the increased charge or polar pendant groups exposed on the interlayer surface.

To demonstrate the film-forming ability of these well-defined star-shaped interlayers, the topography of these TrNBr and TrOH films (3.0 mg/mL in methanol and ethanol, respectively) coated on Si wafer with native SiO$_2$ were studied by AFM (Figure 2a,b). For the TrNBr surface, a relatively smooth surface with a few sharp raised islands was found, giving a small root-mean-square (RMS) roughness of 0.56 nm. Different from its cationic counterpart, the surface of TrOH showed significant aggregation with much more raised islands distributed over the film, leading to an increased RMS
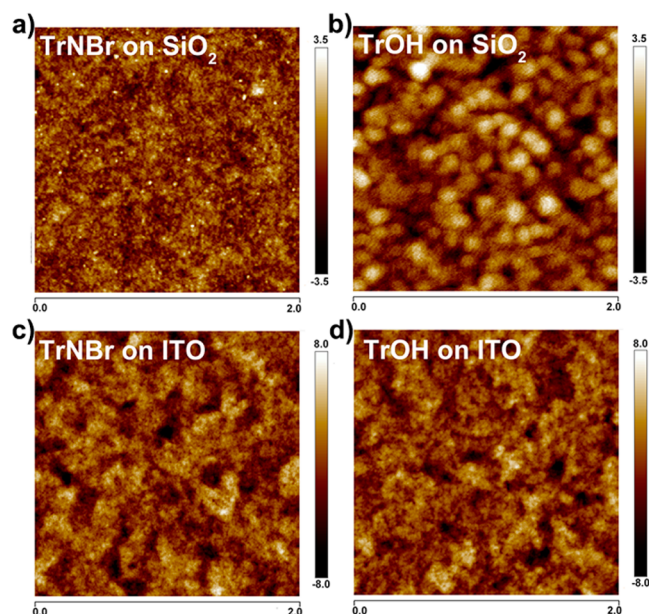
roughness of 0.90 nm. Such self-assembled nanofeatures arise from the vesicle formation in ethanol, resulting from the amphiphilic property of TrOH as well as its molecular structure containing a hydrophobic core and hydrophilic arms (core–shell structure). In conventional BHJ solar cells, surface properties of bottom electrode (e.g., PEDOT:PSS-coated ITO anode) can significantly affect the morphology of the active layer, further dictating the light harvesting, excitons dissociation, charge transport and charge collection.[48] To examine the impact of the star-shaped interlayer films on the morphology of P3HT:ICBA active layer, we monitored their pristine surfaces on ITO. For the ultrathin layers for device fabrication (0.5 mg/mL), the roughness and topography of the interlayer film are predominantly influenced by the ITO (Figure S9a,b, Supporting Information). Hence, the RMS roughness of the TrNBr- and TrOH-coated ITO films are similar to that of bare ITO (3.11 nm). Note that even using a relatively high concentration (3.0 mg/mL), the topography of ITO/interlayer was still influenced by the bottom electrode, leading a reduced RMS of 1.68 and 1.56 nm for TrNBr and TrOH films, respectively (Figure 2c,d). These results indicate that the insertion of the ultrathin film of interlayer in inverted geometry could not have a significant impact on the surface morphology of bottom surface, which is similar to previously reported ITO/ZnO/interlayer cathode surface.[20] Thus, similar surface topography was found on P3HT:ICBA films coated on ITO/TrNBr and ITO/TrOH, with RMS roughness of 3.94 and 3.88 nm, respectively (scan size is 5 $\mu$m × 5 $\mu$m, Figure S10, Supporting Information).

Our previous research has demonstrated that the interlayers (e.g., PFN) show strongly thickness-dependent performance.[22] We first fabricated a series of inverted devices with increasing thickness of both type of interlayers. The inverted devices comprised an ITO-coated glass substrate as the EC electrode, various thickness of interlayers, 250 nm P3HT:ICBA (1:1) photoactive layer, and 2.0 nm evaporated V$_2$O$_5$ capped with 80 nm evaporated silver as the HC electrode. Photocurrent density–voltage ($J$–$V$) characteristics under AM 1.5G irradiation (100 mW/cm$^2$) are shown in Figure 3a. Detailed device parameters are summarized in Tables S4 and S5 (see Supporting Information). No photovoltaic behavior was found in devices with bare ITO and ITO after only alcohol rising. After deposition of a thin film of interlayer, a significantly improved photovoltaic device performance was achieved. For the inverted devices with TrNBr as the EC interlayer, the device performance was really sensitive to interlayer thickness. The highest PCE (5.15%) was achieved in using an ultrathin film of TrNBr (2.40 ± 0.16 nm, 0.13 mg/mL in methanol). For TrOH-based devices, however, the optimized interlayer thickness was 8.7 ± 0.47 nm (0.50 mg/mL in ethanol) with the highest PCE of 4.54%. Further increase of the interlayer thickness did not help the performance of the devices but resulted in the reduction of $J_{SC}$, which can be attributed to the low conductivity of the interlayer and to the reduced EC electrode/interlayer transmittance in UV region. On the other hand, with thinner star-shaped interlayers, an "S-shaped" $J$–$V$ curve with lower fill factor (FF) was found. We suggest that this is because of a nonuniform coverage of interlayer on ITO.

Next, we fabricated inverted devices with optimized spin-casting condition of both interfacial materials at same time. For reference purposes, inverted devices with a sol–gel-derived ZnO electron extraction layer and standard (conventional) devices with configuration of (ITO/PEDOT:PSS/P3HT:IC-
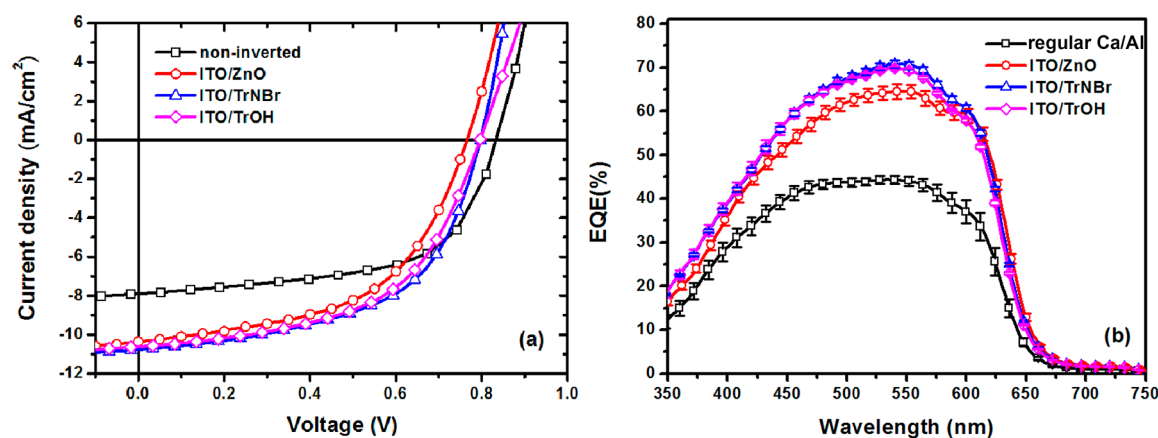


**Figure 2.** AFM surface topography of (a) TrNBr on Si/SiO$_2$ (b) TrOH on Si/SiO$_2$ (c) TrNBr on ITO (d) TrOH on SiO$_2$. Scan size is 2 $\mu$m × 2 $\mu$m, and scan rate is 1 Hz for all images. All the solution concentration was 3 mg/mL, and the spin-casting rate was 2000 rpm.

**Figure 3.** $J-V$ characteristics of solar cells with various interlayer thickness under AM 1.5G irradiation at 100 mW/cm²: (a) TrNBr; (b) TrOH.
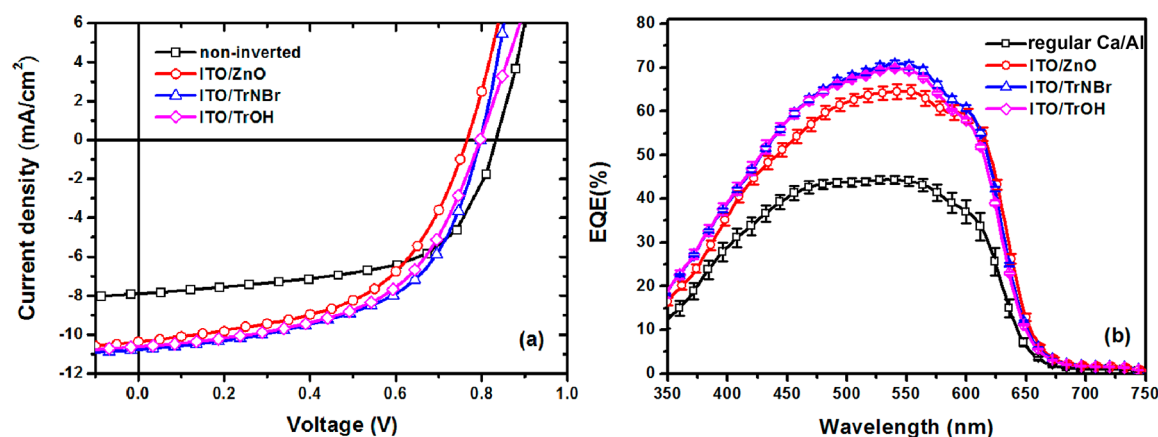


**Figure 4.** (a) $J-V$ characteristics under AM 1.5G irradiation at 100 mW/cm² and (b) EQE spectra of the reference Ca/Al devices (□) and the inverted devices with optimized ZnO (○), TrNBr (△), and TrOH (◇) interlayers.

**Table 1. Electrical Parameters of the Inverted Devices with Various EC Layers and Reference Ca/Al Cathode Devices**

| cathode | $V_{OC}$ (V) | $J_{SC}$ (mA/cm²) | FF (%) | best PCE (%) | averaged PCE (%) | $R_S$ ($\Omega$ cm$^{-2}$)$^a$ |
|---------|-----------|----------------|--------|--------------|------------------|------------------------|
| Ca/Al | 0.83 | 7.88 | 60.3 | 3.94 | 3.84 ± 0.12 | 14.2 |
| ITO/ZnO | 0.77 | 10.30 | 53.1 | 4.21 | 4.17 ± 0.05 | 14.9 |
| ITO/TrNBr | 0.80 | 10.75 | 56.8 | 4.88 | 4.76 ± 0.13 | 10.8 |
| ITO/TrOH | 0.80 | 10.60 | 55.9 | 4.74 | 4.66 ± 0.07 | 16.1 |

$^a$The series resistance ($R_s$) was calculated using $(dJ/dV)^{-1}$.

BA/Ca/Al) were also fabricated. The $J-V$ characteristics of conventional Ca/Al devices and inverted devices with various interfacial layers (ZnO, TrNBr, and TrOH) under AM 1.5G irradiation (100 mW/cm²) are shown in Figure 4a. The main figures of merit of the electrical characterization results are summarized in Table 1. In the reference devices with Ca/Al cathodes, typical open-circuit voltages reach $V_{OC}$ = 0.83 V, short-circuit current densities $J_{SC}$ = 7.88 mA/cm², and FF = 60.3%, giving a PCE = 3.94%. For *i*PSC devices with ZnO, a lower $V_{OC}$ = 0.77 V, a significantly increased $J_{SC}$ = 10.30 mA/cm² and a lower FF = 53.1% were achieved, leading to a PCE of 4.21%, a slightly enhanced relative to the Ca/Al reference device. The use of TrNBr and TrOH as interfacial layer resulted in the increase of the $V_{OC}$ with $V_{OC}$ = 0.80 V, which is a 0.03 V difference in respect to the ZnO-based *i*PSCs. Since the $V_{OC}$ of solar cell is usually determined by the difference in LUMO of acceptor and HOMO of donor, as well as the work function difference between anode and cathode, the increase in

$V_{OC}$ can be attributed to the reduced work function of cathode after TrNBr and TrOH deposition (4.1 eV for TrNBr- and 4.2 eV for TrOH-coated ITO vs 4.4 eV for ZnO). Further, an overall improvement in $J_{SC}$ and FF were achieved compared with ZnO-based interlayer, giving PCE 4.88% for TrNBr and 4.74% for TrOH. The series resistance ($R_S$) of TrOH-based device was 16.1 $\Omega$ cm$^{-2}$, larger than that of TrNBr-based devices (10.8 $\Omega$ cm$^{-2}$). The possible reason is that the optimized thickness of TrOH film (~8.7 nm) was thicker than that of TrNBr films (~2.4 nm), and consequently enhanced the device bulk resistance. Dark $J-V$ characteristics (Figure S11, Supporting Information) verified the good diode behavior of both devices using TrNBr and TrOH interlayers. Although these devices showed strong thickness-dependent performance and high efficiency can only be achieved in ultrathin layers, the efficient electron-extraction ability and low-temperature solution processability are highly attractive. Previous works suggest that this problem can be overcome by using n-type or

high-mobility conjugated backbones.[36,49] Our findings also demonstrate that the optimized thickness for the devices is related to the polar pendent groups.

Figure 4b shows the averaged external quantum efficiency (EQE) spectra for the same devices. In contrast to the conventional Ca/Al devices, all the inverted PSCs exhibited an obvious enhancement in their EQE response across the spectral range of 350−700 nm, in good agreement with the higher $J_{SC}$ of the corresponding $J−V$ curves shown in Figure 4a. The significantly enhanced $J_{SC}$ and EQE response can be attributed to their desired vertical phase separation of the inverted device geometry that is beneficial for charge transport and collection.[11,50] The EQE value of TrNBr- and TrOH-based devices surpasses 70% at ∼550 nm indicating an efficient photon-to-electron conversion. Transmittance spectra show that the sol−gel-derived ZnO film utilized in the iPSC devices exhibits a much stronger incident light energy loss than the star-shaped interlayer in the wavelength range of 300−600 nm (Figure S3, Supporting Information). Thus, the incorporation of the TrNBr and TrOH interlayers in the iPSCs improves the management of the incident light of 300−600 nm, resulting in higher EQEs.

We have compared the stability of the inverted cells in respect to cells with the same photoactive layer but with a conventional device geometry with Ca/Al top EC electrodes and PEDOT:PSS bottom HC-electrodes.[7,8] By avoiding the use of the instable Ca/Al metallic electrodes and of the acidic PEDOT:PSS component, it is found that the stability of the inverted cells is increased. Figure 5 presents the evolution of
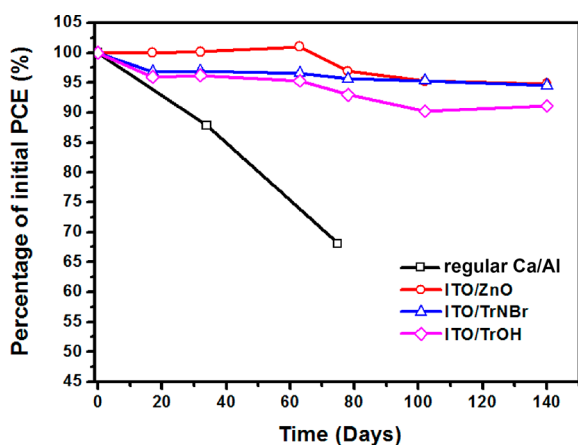


**Figure 5.** Air stability tests on encapsulated P3HT:ICBA devices with regular Ca/Al structure (□) and inverted structure with ITO/ZnO (○), ITO/TrNBr (△), ITO/TrOH (◇) as the cathode.

the device PCE parameter as a function of the efficiency-device storage time for the two sets of devices. Both types of devices were fabricated in a $N_2$-filled glovebox, and they were encapsulated with epoxy/glass slides. During their storage, the devices were kept in the ambient dark condition. The detailed electrical parameters ($J_{SC}$, $V_{OC}$, FF, and PCE) for all devices, as a function of storage time in ambient air, are illustrated in Figure S13 in Supporting Information. For the devices of conventional architecture, the PCE decreased to 68% after staying in ambient conditions for 75 d. In contrast, the PCE of all inverted devices remained to more than 90% of the initial PCE after staying in ambient conditions for 140 d. Previous studies showed that the inverted cells with

polyelectrolyte (both for conjugated or nonconjugated)-based interlayer exhibited comparable device stability to the inorganic buffer layer.[31,51] Particularly for the case of the iPSCs devices functionalized with the star-shaped interlayers, the device stability was much better than the case of the conventional devices but slightly inferior than that of the iPSCs with the ZnO EC interlayer. One possible reason is that these water/alcohol-soluble materials may also be sensitive to the moisture, resulting in slow degradation.

## 4. CONCLUSION

In conclusion, we have successfully fabricated inverted PSCs using TrNBr and TrOH, two monodisperse star-shaped conjugated macroelectrolytes as EC interlayers on the top of ITO electrode substrates. Simple purification process, well-defined structures, good film-forming property as well as the excellent solubility are the attractive advantages of this class of materials. The thickness of each interlayer was tuned carefully, exhibiting an optimized PCE for a thickness of ∼2.4 nm in the case of TrNBr and of ∼8.7 nm in the case of TrOH. Following optimization the solar cell devices delivered a maximum PCE of 4.88% (when TrNBr was used) and of 4.74% (when TrOH was used) with the benefit of avoiding the requirement for reactive metals to be used as EC electrodes, which is an improvement of more than 20% in respect to the reference P3HT:ICBA devices. In comparison to the sol−gel-derived ZnO-based inverted devices, the enhancement in PCE was of 16% and 13%. The utilization of the star-shaped conjugated macroelectrolytes as interlayers in iPSCs resulted in the increase of the device stability when compared with devices of conventional geometry. Advantageously, the solution-processable character of these interlayer materials and their easy processing at low temperatures in ambient atmosphere offer great promise for their incorporation in PSC device fabrication for commercial applications.

## ■ ASSOCIATED CONTENT

### Ⓢ Supporting Information
Synthetic information for TrNBr, optimization of the interlayer thicknesses, further interface property measurements, and detailed device performance. This material is available free of charge via the Internet at http://pubs.acs.org.

## ■ AUTHOR INFORMATION

### Corresponding Authors
*E-mail: iamwylai@njupt.edu.cn. (W.-Y.L.)
*E-mail: iamrdxia@njupt.edu.cn. (R.X.)
*E-mail: p.keivanidis@cut.ac.cy. (P.E.K.)
*E-mail: iamwhuang@njtech.edu.cn. (W.H.)

### Present Addresses
⊥(P.E.K.) Cyprus Univ of Technology, Dept of Mechanical Engineering and Materials Science and Engineering, Dorothea Bldg, fifth floor, 45 Kitiou Kyprianou Str., Limassol 3041, CYPRUS.
∥(T.-L.Y) Dept of Chemistry, Harbin Institute of Technology, Harbin, 150001, P. R. China.

### Notes
The authors declare no competing financial interest.

## ■ ACKNOWLEDGMENTS

## ■ REFERENCES

(1) Hoppe, H.; Sariciftci, N. S. Organic Solar Cells: An Overview. *J. Mater. Res.* **2004**, *19*, 1924−1945.

(2) Wong, K. W.; Yip, H. L.; Luo, Y.; Wong, K. Y.; Lau, W. M.; Low, K. H.; Chow, H. F.; Gao, Z. Q.; Yeung, W. L.; Chang, C. C. Blocking Reactions Between Indium-Tin Oxide and Poly (3,4-Ethylene Dioxythiophene): Poly(Styrene Sulphonate) with a Self-Assembly Monolayer. *Appl. Phys. Lett.* **2002**, *80*, 2788−2790.

(3) Jørgensen, M.; Norrman, K.; Krebs, F. C. Stability/Degradation of Polymer Solar Cells. *Sol. Energy Mater. Sol. Cells* **2008**, *92*, 686−714.

(4) Shuttle, C. G.; O'Regan, B.; Ballantyne, A. M.; Nelson, J.; Bradley, D. D. C.; deMello, J. C.; Durrant, J. R. Experimental Determination of the Rate Law for Charge Carrier Decay in a Polythiophene: Fullerene Solar Cell. *Appl. Phys. Lett.* **2008**, *92*, 093311.

(5) Brabec, C. J.; Gowrisanker, S.; Halls, J. J. M.; Laird, D.; Jia, S. J.; Williams, S. P. Polymer-Fullerene Bulk-Heterojunction Solar Cells. *Adv. Mater.* **2010**, *22*, 3839−3856.

(6) Xia, R.; Al-Hashimi, M.; Tsoi, W. C.; Heeney, M.; Bradley, D. D. C.; Nelson, J. Fused Pyrrolo[3,2-d:4,5-d′]bisthiazole-Containing Polymers for Using in High-Performance Organic Bulk Heterojunction Solar Cells. *Sol. Energy Mater. Sol. Cells* **2012**, *96*, 112−116.

(7) Kawano, K.; Pacios, R.; Poplavskyy, D.; Nelson, J.; Bradley, D. D. C.; Durrant, J. R. Degradation of Organic Solar Cells Due to Air Exposure. *Sol. Energy Mater. Sol. Cells* **2006**, *90*, 3520−3530.

(8) Krebs, F. C.; Norrman, K. Analysis of the Failure Mechanism for a Stable organic Photovoltaic During 10000 h of Testing. *Prog. Photovoltaics* **2007**, *15*, 697−712.

(9) Scharber, M. C.; Mühlbacher, D.; Koppe, M.; Denk, P.; Waldauf, C.; Heeger, A. J.; Brabec, C. J. Design Rules for Donors in Bulk-Heterojunction Solar Cells - Towards 10% Energy-Conversion Efficiency. *Adv. Mater.* **2006**, *18*, 789−794.

(10) Kim, Y.; Cook, S.; Tuladhar, S. M.; Choulis, S. A.; Nelson, J.; Durrant, J. R.; Bradley, D. D. C.; Giles, M.; McCulloch, I.; Ree, C. M. A Strong Regioregularity Effect in Self-Organizing Conjugated Polymer Films and High-Efficiency Polythiophene: Fullerene Solar Cells. *Nat. Mater.* **2006**, *5*, 197−203.

(11) Campoy-Quiles, M.; Ferenczi, T.; Agostinelli, T.; Etchegoin, P. G.; Kim, Y.; Anthopoulos, T. D.; Stavrinou, P. N.; Bradley, D. D. C.; Nelson, J. Morphology Evolution via Self-Organization and Lateral and Vertical Diffusion in Polymer: Fullerene Solar Cell Blends. *Nat. Mater.* **2008**, *7*, 158−164.

(12) Shrotriya, V.; Li, G.; Yao, Y.; Chu, C.-W.; Yang, Y. Effects of C-70 Derivative in Low Band Gap Polymer Photovoltaic Devices: Spectral Complementation and Morphology Optimization. *Appl. Phys. Lett.* **2006**, *88*, 073508.

(13) Kyaw, A. K. K.; Sun, X. W.; Jiang, C. Y.; Lo, G. Q.; Zhao, D. W.; Kwong, D. L. An Inverted Organic Solar Cell Employing a Sol-Gel Derived ZnO Electron Selective Layer and Thermal Evaporated MoO$_3$ Hole Selective Layer. *Appl. Phys. Lett.* **2008**, *93*, 221107.

(14) Sun, Y.; Seo, J. H.; Takacs, C. J.; Seifter, J.; Heeger, A. J. Inverted Polymer Solar Cells Integrated with a Low-Temperature-Annealed Sol-Gel-Derived ZnO Film as an Electron Transport Layer. *Adv. Mater.* **2011**, *23*, 1679−1683.

(15) Waldauf, C.; Morana, M.; Denk, P.; Schilinsky, P.; Coakley, K.; Choulis, S. A.; Brabec, C. J. Highly Efficient Inverted Organic Photovoltaics Using Solution Based Titanium Oxide as Electron Selective Contact. *Appl. Phys. Lett.* **2006**, *89*, 233517.

(16) Liu, J.; Shao, S.; Fang, G.; Meng, B.; Xie, Z.; Wang, L. High-Efficiency Inverted Polymer Solar Cells with Transparent and Work-Function Tunable MoO$_3$-Al Composite Film as Cathode Buffer Layer. *Adv. Mater.* **2012**, *24*, 2774−2779.

(17) Huang, J.; Li, G.; Yang, Y. A Semi-Transparent Plastic Solar Cell Fabricated by a Lamination Process. *Adv. Mater.* **2008**, *20*, 415−419.

(18) Li, G.; Chu, C.-W.; Shrotriya, V.; Huang, J.; Yang, Y. Efficient Inverted Polymer Solar Cells. *Appl. Phys. Lett.* **2006**, *88*, 253503.

(19) Hsieh, C.-H.; Cheng, Y.-J.; Li, P.-J.; Chen, C.-H.; Dubosc, M.; Liang, R.-M.; Hsu, C.-S. Highly Efficient and Stable Inverted Polymer Solar Cells Integrated with a Cross-Linked Fullerene Material as an Interlayer. *J. Am. Chem. Soc.* **2010**, *132*, 4887−4893.

(20) Kyaw, A. K. K.; Wang, D. H.; Gupta, V.; Zhang, J.; Chand, S.; Bazan, G. C.; Heeger, A. J. Efficient Solution-Processed Small-Molecule Solar Cells with Inverted Structure. *Adv. Mater.* **2013**, *25*, 2397−2402.

(21) Duan, C. H.; Zhang, K.; Zhong, C. M.; Huang, F.; Cao, Y. Recent Advances in Water/Alcohol-Soluble π-conjugated Materials: New Materials and Growing Applications in Solar Cells. *Chem. Soc. Rev.* **2013**, *42*, 9071−9104.

(22) Xia, R.; Leem, D.-S.; Kirchartz, T.; Spencer, S.; Murphy, C.; He, Z. C.; Wu, H. B.; Su, S. J.; Cao, Y.; Kim, J. S.; deMello, J. C.; Bradley, D. D. C.; Nelson, J. Investigation of a Conjugated Polyelectrolyte Interlayer for Inverted Polymer:Fullerene Solar Cells. *Adv. Energy Mater.* **2013**, *3*, 718−723.

(23) Liu, F.; Page, Z. A.; Duzhko, V. V.; Russell, T. P.; Emrick, T. Conjugated Polymeric Zwitterions as Efficient Interlayers in Organic Solar Cells. *Adv. Mater.* **2013**, *25*, 6868−6873.

(24) Lu, H.-H.; Ma, Y.-S.; Yang, N.-J.; Lin, G.-H.; Wu, Y.-C.; Chen, S.-A. Creating a Pseudometallic State of K$^+$ by Intercalation into 18-Crown-6 Grafted on Polyfluorene as Electron Injection Layer for High Performance PLEDs with Oxygen- and Moisture-Stable Al Cathode. *J. Am. Chem. Soc.* **2011**, *133*, 9634−9637.

(25) Ye, T. L.; Zhu, M. R.; Chen, J. S.; Fu, Q.; Zhao, F. C.; Shi, C. S.; Hu, Y.; Ma, D. G.; Yang, C. L. Efficient Electron Injection Layer Based on Thermo-Cleavable Materials for Inverted Bottom-Emission Polymer Light Emitting Diodes. *J. Mater. Chem.* **2012**, *22*, 6413−6418.

(26) Xu, W.; Zhang, X.; Hu, Q.; Zhao, L.; Teng, X.; Lai, W.-Y.; Xia, R.; Nelson, J.; Huang, W.; Bradley, D. D. C. Fluorene-Based Cathode Interlayer Polymers for High Performance Solution Processed Organic Optoelectronic Devices. *Org. Electron.* **2014**, *15*, 1244−1253.

(27) Zheng, H.; Zheng, Y.; Liu, N.; Ai, N.; Wang, Q.; Wu, S.; Zhou, J.; Hu, D.; Yu, S.; Han, S.; Xu, W.; Luo, C.; Meng, Y.; Jiang, Z.; Chen, Y.; Li, D.; Huang, F.; Wang, J.; Peng, J.; Cao, Y. All-Solution Processed Polymer Light-Emitting Diode Displays. *Nat. Commun.* **2013**, *4*, 1971−1977.

(28) He, Z. C.; Zhong, C. M.; Su, S. J.; Xu, M.; Wu, H. B.; Cao, Y. Enhanced Power-Conversion Efficiency in Polymer Solar Cells Using an Inverted Device Structure. *Nat. Photonics* **2012**, *6*, 591−595.

(29) Yang, T.; Wang, M.; Duan, C.; Hu, X.; Huang, L.; Peng, J.; Huang, F.; Gong, X. Inverted Polymer Solar Cells with 8.4% Efficiency by Conjugated Polyelectrolyte. *Energy Environ. Sci.* **2012**, *5*, 8208−8214.

(30) Choi, H.; Park, J. S.; Jeong, E.; Kim, G.-H.; Lee, B. R.; Kim, S. O.; Song, M. H.; Woo, H. Y.; Kim, J. Y. Combination of Titanium Oxide and a Conjugated Polyelectrolyte for High-Performance Inverted-Type Organic Optoelectronic Devices. *Adv. Mater.* **2011**, *23*, 2759−2763.

(31) Sun, J. M.; Zhu, Y. X.; Xu, X. F.; Lan, L. F.; Zhang, L. J.; Cai, P.; Chen, J. W.; Peng, J. B.; Cao, Y. High Efficiency and High $V_{OC}$ Inverted Polymer Solar Cells Based on a Low-Lying HOMO Polycarbazole Donor and a Hydrophilic Polycarbazole Inter Layer on ITO Cathode. *J. Phys. Chem. C* **2012**, *116*, 14188−14198.

(32) Zhou, Y.; Li, F.; Barrau, S.; Tian, W.; Inganäs, O.; Zhang, F. Inverted and Transparent Polymer Solar Cells Prepared with Vacuum-Free Processing. *Sol. Energy Mater. Sol. Cells* **2009**, *93*, 497−500.

(33) Seo, J. H.; Nguyen, T.-Q. Electronic Properties of Conjugated Polyelectrolyte Thin Films. *J. Am. Chem. Soc.* **2008**, *130*, 10042−10043.

(34) Zhou, Y.; Fuentes-Hernandez, C.; Shim, J.; Meyer, J.; Giordano, A. J.; Li, H.; Winget, P.; Papadopoulos, T.; Cheun, H.; Kim, J.; Fenoll, M.; Dindar, A.; Haske, W.; Najafabadi, E.; Khan, T. M.; Sojoudi, H.; Barlow, S.; Graham, S.; Brédas, J.-L.; Marder, S. R.; Kahn, A.; Kippelen, B. A Universal Method to Produce Low-Work Function Electrodes for Organic Electronics. *Science* **2012**, *336*, 327−332.

(35) Chen, Y.; Jiang, Z. T.; Gao, M.; Watkins, S. E.; Lu, P.; Wang, H. Q.; Chen, X. W. Efficiency Enhancement for Bulk Heterojunction Photovoltaic Cells *via* Incorporation of Alcohol Soluble Conjugated Polymer Interlayer. *Appl. Phys. Lett.* **2012**, *100*, 203304.

(36) Liu, S.; Zhang, K.; Lu, J.; Zhang, J.; Yip, H.-L.; Huang, F.; Cao, Y. High-Efficiency Polymer Solar Cells *via* the Incorporation of an Amino-Functionalized Conjugated Metallopolymer as a Cathode Interlayer. *J. Am. Chem. Soc.* **2013**, *135*, 15326−15329.

(37) Kanibolotsky, A. L.; Perepichka, I. F.; Skabara, P. J. Star-Shaped π-Conjugated Oligomers and Their Applications in Organic Electronics and Photonics. *Chem. Soc. Rev.* **2010**, *39*, 2695−2728.

(38) Lo, S. C.; Burn, P. L. Development of Dendrimers: Macromolecules for use in Organic Light-Emitting Diodes and Solar Cells. *Chem. Rev.* **2007**, *107*, 1097−1116.

(39) Lai, W. Y.; Zhu, R.; Fan, Q.-L.; Hou, L.-T.; Cao, Y.; Huang, W. Monodisperse Six-Armed Triazatruxenes: Microwave-Enhanced Synthesis and Highly Efficient Pure-Deep-Blue Electroluminescence. *Macromolecules* **2006**, *39*, 3707−3709.

(40) Xia, R.; Lai, W. Y.; Levermore, P. A.; Huang, W.; Bradley, D. D. C. Low-Threshold Distributed-Feedback Lasers Based on Pyrene-Cored Starburst Molecules with 1,3,6,8-Attached Oligo(9,9-Dialkyl-fluorene) Arms. *Adv. Funct. Mater.* **2009**, *19*, 2844−2850.

(41) Lai, W. Y.; Xia, R.; He, Q.-Y.; Levermore, P. A.; Huang, W.; Bradley, D. D. C. Enhanced Solid-State Luminescence and Low-Threshold Lasing from Starburst Macromolecular Materials. *Adv. Mater.* **2009**, *21*, 355−360.

(42) Skabara, P. J.; Arlin, J.-B.; Geerts, Y. H. Close Encounters of the 3D Kind Exploiting High Dimensionality in Molecular Semiconductors. *Adv. Mater.* **2013**, *25*, 1948−1954.

(43) Xu, W.; Lai, W.-Y.; Hu, Q.; Teng, X. Y.; Zhang, X. W.; Huang, W. A Hydrophilic Monodisperse Conjugated Starburst Macromolecule with Multidimensional Topology as Electron Transport/Injection Layer for Organic Electronics. *Polym. Chem.* **2014**, *5*, 2942−2950.

(44) Zhao, G. J.; He, Y. J.; Li, Y. F. 6.5% Efficiency of Polymer Solar Cells Based on Poly(3-hexylthiophene) and Indene-C-60 Bisadduct by Device Optimization. *Adv. Mater.* **2010**, *22*, 4355−4358.

(45) Huang, F.; Wu, H. B.; Wang, D. L.; Yang, W.; Cao, Y. Novel Electroluminescent Conjugated Polyelectrolytes Based on Polyfluorene. *Chem. Mater.* **2004**, *16*, 708−716.

(46) Huang, F.; Niu, Y.-H.; Zhang, Y.; Ka, J.-W.; Liu, M. S.; Jen, A. K. Y. A Conjugated, Neutral Surfactant as Electron-Injection Material for High-Efficiency Polymer Light-Emitting Diodes. *Adv. Mater.* **2007**, *19*, 2010−2014.

(47) Meyer, J.; Zilberberg, K.; Riedl, T.; Kahn, A. Electronic Structure of Vanadium Pentoxide: An Efficient Hole Injector for Organic Electronic Materials. *J. Appl. Phys.* **2011**, *110*, 033710.

(48) Li, S. S.; Tu, K. H.; Lin, C. C.; Chen, C. W.; Chhowalla, M. Solution-Processable Graphene Oxide as an Efficient Hole Transport Layer in Polymer Solar Cells. *ACS Nano* **2010**, *4*, 3169−3174.

(49) Li, C.-Z.; Chang, C.-Y.; Zang, Y.; Ju, H.-X.; Chueh, C.-C.; Liang, P.-W.; Cho, N.; Ginger, D. S.; Jen, A. K.-Y. Suppressed Charge Recombination in Inverted Organic Photovoltaics via Enhanced Charge Extraction by Using a Conductive Fullerene Electron Transport Layer. *Adv. Mater.* **2014**, *26*, 6262−6267.

(50) Xu, Z.; Chen, L.-M.; Yang, G.; Huang, C.-H.; Hou, J.; Wu, Y.; Li, G.; Hsu, C.-S.; Yang, Y. Vertical Phase Separation in Poly(3-hexylthiophene): Fullerene Derivative Blends and Its Advantage for Inverted Structure Solar Cells. *Adv. Funct. Mater.* **2009**, *19*, 1227−1234.

(51) Cai, P.; Zhong, S.; Xu, X.; Chen, J.; Chen, W.; Huang, F.; Ma, Y.; Cao, Y. Using Ultra-High Molecular Weight Hydrophilic Polymer as Cathode Interlayer for Inverted Polymer Solar Cells: Enhanced Efficiency and Excellent Air-Stability. *Sol. Energy Mater. Sol. Cells* **2014**, *123*, 104−111.